



HAL
open science

Atom Probe Tomography Interlaboratory Study on Clustering Analysis in Experimental Data Using the Maximum Separation Distance Approach

Yan Dong, Auriane Etienne, Alex Frolov, Svetlana Fedotova, Katsuhiko Fujii, Koji Fukuya, Constantinos Hatzoglou, Evgenia Kuleshova, Kristina Lindgren, Andrew London, et al.

► To cite this version:

Yan Dong, Auriane Etienne, Alex Frolov, Svetlana Fedotova, Katsuhiko Fujii, et al.. Atom Probe Tomography Interlaboratory Study on Clustering Analysis in Experimental Data Using the Maximum Separation Distance Approach. *Microscopy and Microanalysis*, 2019, Special Issue 2 (Atom Probe Tomography and Microscopy APT&M 2018), 25, pp.356-366. 10.1017/S1431927618015581 . hal-02106727

HAL Id: hal-02106727

<https://hal.science/hal-02106727v1>

Submitted on 29 May 2020

HAL is a multi-disciplinary open access archive for the deposit and dissemination of scientific research documents, whether they are published or not. The documents may come from teaching and research institutions in France or abroad, or from public or private research centers.

L'archive ouverte pluridisciplinaire **HAL**, est destinée au dépôt et à la diffusion de documents scientifiques de niveau recherche, publiés ou non, émanant des établissements d'enseignement et de recherche français ou étrangers, des laboratoires publics ou privés.

Atom Probe Tomography Interlaboratory Study on Clustering Analysis in Experimental Data Using the Maximum Separation Distance Approach

Yan Dong¹, Auriane Etienne², Alex Frolov³, Svetlana Fedotova³, Katsuhiko Fujii⁴, Koji Fukuya⁴, Constantinos Hatzoglou², Evgenia Kuleshova³, Kristina Lindgren⁵, Andrew London⁶, Anabelle Lopez⁷, Sergio Lozano-Perez⁸, Yuichi Miyahara⁹, Yasuyoshi Nagai¹⁰, Kenji Nishida⁹, Bertrand Radiguet², Daniel K. Schreiber¹¹, Naoki Soneda⁹, Mattias Thuvander⁵, Takeshi Toyama¹⁰, Jing Wang¹¹, Faiza Sefta¹², Peter Chou¹³ and Emmanuelle A. Marquis^{1*}

¹Department of Materials Science and Engineering, University of Michigan, Ann Arbor, MI 48109, USA; ²Normandie Univ, UNIROUEN, INSA Rouen, CNRS, Groupe de Physique des Matériaux, F-76000 Rouen, France; ³National Research Center 'Kurchatov Institute', Pl. Kurchatova, 123 182 Moscow, Russian Federation; ⁴Institute of Nuclear Safety System Inc., 64 Sata, Mihama 919-1205, Japan; ⁵Department of Physics, Chalmers University of Technology, SE-412 96, Göteborg, Sweden; ⁶United Kingdom Atomic Energy Authority, Culham Science Centre, Abingdon, Oxon, OX14 3DB, UK; ⁷DEN-Service d'Etudes des Matériaux Irradiés, CEA, Université Paris-Saclay, F-91191, Gif-sur-Yvette, France; ⁸Department of Materials, University of Oxford, Parks Road, Oxford OX1 3PH, UK; ⁹Materials Science Research Laboratory, Central Research Institute of Electric Power Industry, Yokosuka, Japan; ¹⁰The Oarai Center, Institute for Materials Research, Tohoku University, Oarai, Ibaraki 311-1313, Japan; ¹¹Energy and Environment Directorate, Pacific Northwest National Laboratory, Richland, WA 99352, USA; ¹²Departement Métallurgie, EDF—R&D, Avenue des Renardières—Ecuelles, 77818 Moret-sur-Loing, France and ¹³Electric Power Research Institute, Palo Alto, CA, 94304, USA

Abstract

We summarize the findings from an interlaboratory study conducted between ten international research groups and investigate the use of the commonly used maximum separation distance and local concentration thresholding methods for solute clustering quantification. The study objectives are: to bring clarity to the range of applicability of the methods; identify existing and/or needed modifications; and interpretation of past published data. Participants collected experimental data from a proton-irradiated 304 stainless steel and analyzed Cu-rich and Ni-Si rich clusters. The datasets were also analyzed by one researcher to clarify variability originating from different operators. The Cu distribution fulfills the ideal requirements of the maximum separation method (MSM), namely a dilute matrix Cu concentration and concentrated Cu clusters. This enabled a relatively tight distribution of the cluster number density among the participants. By contrast, the group analysis of the Ni-Si rich clusters by the MSM was complicated by a high Ni matrix concentration and by the presence of Si-decorated dislocations, leading to larger variability among researchers. While local concentration filtering could, in principle, tighten the results, the cluster identification step inevitably maintained a high scatter. Recommendations regarding reporting, selection of analysis method, and expected variability when interpreting published data are discussed.

Keywords: atom probe tomography, cluster analysis, maximum separation

(Received 17 August 2018; revised 16 October 2018; accepted 12 November 2018)

Introduction

Atom probe tomography (APT) has become a technique of reference for compositional analysis of nanoscale phases, interfacial segregation, and solute clustering. APT generates three-dimensional reconstructions of atomic position and elemental identity from needle-shaped specimens using a combination of field evaporation, time-of-flight mass spectrometry, single-atom and position-sensitive detection, and a tomographic reconstruction algorithm. With these attributes, APT has played an important role in the characterization of microstructural changes in

irradiated materials that are difficult to describe by more broadly applied electron microscopy techniques. For example, APT has been used to clarify our understanding of microstructural evolution (Styman et al., 2015; Shu et al., 2018), irradiation-induced hardening (Takeuchi et al., 2010), and inform models used in surveillance programs (Auger et al., 2000; Miller et al., 2000; Miller & Russell, 2007; Toyama et al., 2007; Meslin et al., 2010; Kuramoto et al., 2013; Gurovich et al., 2015; Styman et al., 2015; Edmondson et al., 2016). Within the nuclear energy community, APT has not only been used for fundamental understanding of microstructural degradation, but also for large scale surveillance programs entailing retrieval and analysis of samples from existing nuclear plants (Pareige et al., 1997; Miller et al., 2000; Kuramoto et al., 2013; Miller et al., 2013; Toyama et al., 2014). In this respect, a key advantage of APT is the very small volume required for analysis, typically contained within a $2 \times 2 \times 2 \mu\text{m}^3$ cube, mitigating the

*Author for correspondence: Emmanuelle A. Marquis, E-mail: emarq@umich.edu
Cite this article: Dong Y et al (2019) Atom Probe Tomography Interlaboratory Study on Clustering Analysis in Experimental Data Using the Maximum Separation Distance Approach. *Microsc Microanal*. doi:10.1017/S1431927618015581

issues associated with radioactive material handling that can be a significant issue for irradiated stainless steel components that are located closer to the core.

The continued value of APT as a core analysis technique requires reliable and reproducible quantification of the collected data. Nuclear plant safety and the design of future reactors rely on accurate long-term prediction of, not only the microstructural evolution during service, but also the corresponding mechanical properties of the material. A major contribution to the evolution of mechanical properties of most alloys in service within the nuclear industry is the irradiation-induced formation of solute clusters, and while mechanical properties can be challenging to assess, APT analysis of these microstructures is a far simpler avenue (Miller & Russell, 2007). Therefore, quantitative and accurate clustering analysis from APT data is a key step in the establishment of reliable microstructure/property relationships, as well as microstructure evolution models. It is not a trivial step however. As with any other experimental method, analysis of the APT data requires an understanding of the mechanisms of data generation along with possible limitations and artifacts, a definition of the objects of interest, and a data processing method to quantify the objects. Data generation is beyond the scope of this paper, and we will refer the reader to existing monographs (Gault et al., 2012b). However, it is important to recognize that the physical processes controlling movement and evaporation of atoms under an applied electric field, and the limitations inherent to the reconstruction algorithms, may result in artifacts and errors in the reconstructed data, with significant consequences on the outcome of the data analysis procedure. Obvious artifacts manifest themselves as variations in the reconstructed atomic density and variations in solute concentrations that depend on crystallographic orientation. Additional sources of uncertainty may be less evident. A number of mechanisms have been identified with significant effects on the spatial and chemical accuracy of the reconstructed data, which includes localized hopping of atoms on the sample surface prior to evaporation (roll-up motion) (Vaugh et al., 1876), longer range surface diffusion (Gault et al., 2012a), local changes in the field distribution, particularly near terrace edges (Rose, 1956; Vurpillot et al., 2000b), nonuniform evaporation due to evaporation field differences between phases or crystallographic orientations (Miller & Hetherington, 1991; Vurpillot et al., 2000a), or detection biased against multiple events (Saxey, 2011). Beyond possible limitations due to the physics of the technique and algorithm by which data are reconstructed, treatment of the data presents its own challenges.

The analysis of solute clustering from APT data obtained from nuclear materials has largely relied on density based methods, and more specifically the so-called *maximum separation method* (MSM) approach (Heinrich et al., 2003; Vaumousse et al., 2003) and its variation, local concentration thresholding (LCT) (Meslin et al., 2013). Within the MSM, a solute cluster is defined as a region where solute atoms are spatially closer to one another than they would be when randomly distributed. The MSM relies on three parameters: k , d_{\max} , and N_{\min} . The order, k , defines the order of the nearest neighbor considered. If the k th nearest neighbor is within the critical distance, d_{\max} , of another solute atom, then these atoms, and of course the lower order neighbors, are part of the same cluster (Heinrich et al., 2003; Vaumousse et al., 2003; Cerezo & Davin, 2007; Stephenson et al., 2007). A cluster requires a minimum number of solute atoms, N_{\min} , to reduce the count of statistically random occurrences of a few solute atoms being close together. The variant method with LCT employs an analysis of

the local solute concentration to reduce statistical noise from random variations in the data. Clustered atoms require that the local concentration or density of neighboring solutes being higher than a critical threshold concentration, C_{th} or number of atoms, N_{th} (Blavette & Chambreland, 1986; Radiguet et al., 2007; Hyde et al., 2009), where “locality” is given as the volume defined by a sphere, number of nearest neighbor, or voxel, and by a minimum number of solute atoms, N_{\min} . A combination of both methods, also called the “iso-position method” (IPM) as coded within the proprietary software used by the University of Rouen, filters solute atoms with a high local concentration before applying an envelope algorithm [6] or MSM to increase the contrast between clusters and matrix (Meslin et al., 2013; Chen et al., 2014; Lefebvre et al., 2016; Hyde et al., 2017).

In either of the two approaches described above, the selection of the analysis parameters is an important step that can significantly modify the outcome of the analysis. A number of studies have been dedicated to defining objective methods of selection. Using a small set of synthetic microstructures, Hyde et al. found that d_{\max} has the largest influence on the outcome (Hyde et al., 2011). The selection of N_{\min} and the resulting error on the number density of precipitates were addressed by Cerezo & Davin (2007) by comparing the outcomes of the cluster search algorithm performed on an experimental dataset and on a random solid solution. The N_{\min} value should minimize the number of random occurrences in the matrix (Vaumousse et al., 2003; Cerezo & Davin, 2007) and Styman et al. refined this step by adding a comparison of cluster compositions in the experimental and randomized datasets (Styman et al., 2013). Shuffling the mass-to-charge values is used to create a mass-randomized atom probe dataset (Cerezo & Davin, 2007)—as this retains the correct overall composition—while keeping the detected positions, although one should consider the multiplicity of possible random datasets giving rise to a range of possible N_{\min} values (Williams et al., 2013). Different methods have been proposed for the objective selection of a d_{\max} value. These have relied largely on the interpretation of the distribution of nearest neighbor distances (NND) to enable a selection of d_{\max} that attempts to minimize the inclusion of random clusters, and the errant splitting or merging of clusters (Marceau et al., 2011). As a variation on this approach, Jäggle et al. proposed to re-examine the NNDs by fitting the part of the distribution pertaining to the matrix rather than selecting a d_{\max} value based on the comparison with a randomized dataset (Jäggle et al., 2014). Alternatively, Kolli & Seidman suggested using the variations of the number of clusters to find an optimum value (Kolli & Seidman, 2007). Following observations that optimized values of d_{\max} and N_{\min} are correlated (Hyde et al., 2011), Williams et al. proposed to compare the observed number of clusters with the expected number of cluster in a randomized dataset by sweeping through a wide range of the parameter space (Williams et al., 2013).

Despite the number of proposed methods to objectively select parameters, the challenge remains that no standardized approach to the analysis of solute clusters can be applied, as no single method works for all microstructures of interest (Ceguerra et al., 2010). As illustrated below, the MSM is well-suited for microstructures where the solute density contrast between clusters and matrix is significant, but fails when that contrast is reduced. Therefore, not all microstructures will be amenable to this technique and its limitations require clarification. In addition, incomplete reporting of the analysis procedures is apparent in the open literature, raising concerns for the interpretation, validity, and

reproducibility of the reported measurements. In particular, the absence of details and error or variability analyses can limit the reader's assessment of data quality and of appropriateness for comparison against other work or future work.

To address these concerns, the present interlaboratory study, conducted among ten international research groups, aims at bringing awareness about limitations of the commonly used algorithms, the importance of community testing and vetting of data analysis algorithms, and the ethical question about reproducibility and transparency when reporting data. We feel that transparency is a particularly important issue as APT grows as a core analytical technique for nuclear materials with its corresponding financial and social consequences. Through systematic testing of the traditional cluster search methods when applied to a prototypical stainless steel microstructure, the study clarifies the range of applications suitable to the use of this algorithm, leading to recommendations for best practices in the use of these methods, and a template for reporting data that will assist future researchers in need of re-interpretation of published data. Variations on these cluster-finding algorithms, such as Fourier transform and auto-correlation functions (Vurpillot et al., 2004), pair correlation functions (De Geuser et al., 2006; Couturier et al., 2016), Delaunay tessellation (Lefebvre et al., 2011), iso-concentration surfaces and proximity histograms (Hellman et al., 2000), frequency distributions (Moody et al., 2008), and more recently Gaussian mixture models (Zelenty et al., 2017) have also been developed for and/or applied to the detection and analysis of solute clusters in APT data; however these are beyond the scope of this interlaboratory study.

In a first stage of the study, participants were provided with synthetic datasets aimed at testing the algorithms and development of a protocol for data reporting (Marquis et al., 2017). Following the first round of analysis of synthetic datasets, participants were then asked to collect and analyze experimental data. Here we focused on proton irradiated 304 steel, selected for the presence of two populations of clusters, namely Cu clusters and Ni-Si clusters. To limit the number of sources of variables, one operator performed multiple liftouts by conventional focused ion beam (FIB) methods (Thompson et al., 2007) from one grain and mounted APT blanks onto Si microposts. The blanks were shipped to the participant laboratories who individually performed final tip sharpening, data collection, and data analysis. All of the collected data were also shared with and analyzed by a single operator. The resulting measurements are presented after a synopsis of the previous interlaboratory discussions on synthetic data to give context for the current measurements. The analyses by a single operator and by individual participants are organized by features, namely Cu-rich clusters, Ni- and Si-rich clusters, and dislocation loops as identified by Si segregation. Findings and recommendations that emerged from this interlaboratory study are discussed.

Methods

Summary of Phase I

Participants independently analyzed four synthetic datasets created to identify and measure number density, size, and composition of the cluster populations and to test the reproducibility, accuracy, and validity of the MSM, LCT, and IPM methods. The first stage of this round-robin experiment highlighted the ability of the MSM to reliably find clusters in microstructures

with highly concentrated solute clusters in a solute dilute matrix. For datasets with higher matrix solute concentrations, the IPM was recommended—this method reduces the microstructure to one with high contrast, where the maximum separation method (MSM) can then be applied more reliably. Discussions among participants emphasized the need for thorough reporting of the analysis methods, including detailed justification of the method and parameters used within scientific publications. The information is not only essential for the reproducibility of the results, but also ensures that the data presented can be accurately interpreted by future researchers. Minimum information would include:

- Core atoms (or relevant ranges within the mass to charge state ratio spectrum).
- Analysis method and any variation from the common approach.
- Generation of a randomized dataset for comparison with experimental data to select analysis parameters.
- Sensitivity analysis or some measure of the dependence of the results with the parameters as an estimation of uncertainty.
- Method used to define N_{\min} .
- Specification of how edge clusters are counted and how many are found.

These findings are comprehensively presented in Marquis et al. (2017).

Sample and Procedures

For the second round of experiments targeting experimental data, small volumes were extracted by a liftout method, using a Thermo Fisher (formerly FEI) Helios 650 Nanolab scanning electron microscope (SEM) and FIB instrument, from a 304 stainless steel that had been proton-irradiated at 360°C to 10 dpa. The dpa value damage profiles for the irradiations had previously been estimated using Stopping and Range of Ions in Matter (SRIM) with the full cascade option (Jiao & Was, 2011). This material was selected for the presence of two populations of clusters, namely Cu clusters and Ni-Si clusters. Figure 1 confirms that all specimens were extracted from one single grain. Each participant received two mounted specimens and was responsible for sharpening and collecting APT data using the instrument available to them. All participants used Cameca LEAP 4000X HR instruments, with the exception of two participants, one using a Cameca LEAP 3000X HR, and another a Cameca LEAP 5000 XR instrument. Instructions specified data collection conditions, nominally at a sample temperature of 50 K and use of voltage pulsing. An additional dataset was collected in laser mode on a LEAP 5000 XR instrument, using a sample temperature of 50 K and a very high laser pulse energy of 0.2–0.3 nJ to simulate “non-ideal” data collection conditions.

Datasets

Two sets of analyses were conducted. One set was performed by the same operator analyzing all datasets collected in voltage mode (13 in total). The other consisted of each operator analyzing the dataset collected at their home institution (14 in total, including the dataset collected in laser pulsing mode). In the case of the single operator, reconstructed volumes were generated using Cameca's IVAS 3.8.0 software. Reconstruction parameters (kf and ICF) were selected such that radial and axial density variations were minimized (Haley, 2010) and Ni clusters have close

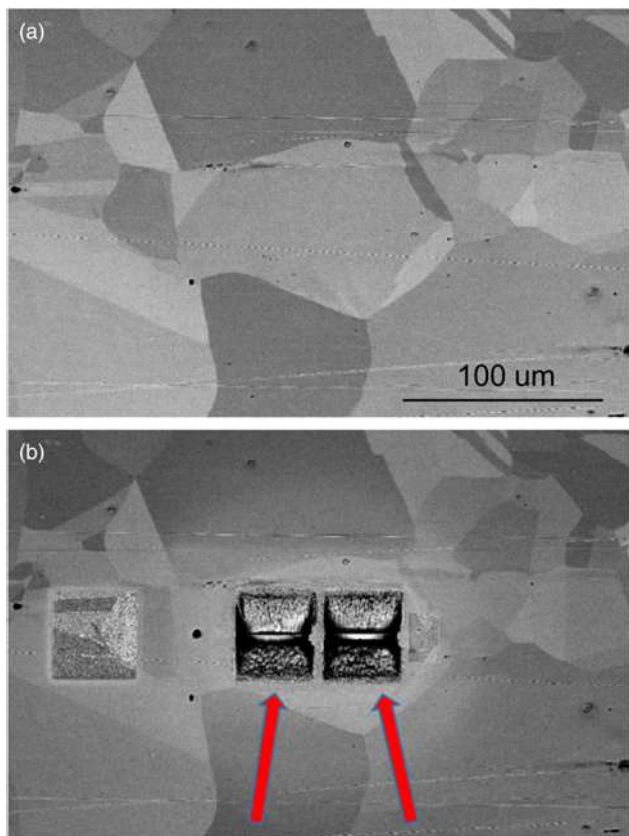


Fig. 1. SEM images of the selected location before sample preparation (a) and showing the positions of the two liftouts used to make samples distributed to the participants within the same grain (b).

to a spherical shape. Reconstructions of the datasets by the different operators were also performed within IVAS software, but followed somewhat different criteria that included using SEM images of the sample shape to inform the shank angle evolution, using plane spacing assuming that a (111) pole is visible within the data, so that Cu clusters would be spherical. Data collection and reconstruction conditions are summarized in Table 1 and both sets of reconstructions are displayed in Figure 2.

Results

It is worth reminding the reader that the analysis methods will only focus on the MSM as implemented in the software package IVAS, a LCT prior to the use of MSM, and IPM as implemented in the University of Rouen software package.

Cu Clusters

The measured Cu concentration in the reconstructed datasets was within the range 0.29–0.38 at% (Fig. 3a). The variations in concentration may be significant considering that counting errors are of the order of 0.002–0.003 at%. As a result of irradiation, a high number density of nanometer scale dense Cu clusters was observed in all datasets. Here, we focus on the quantification of the cluster number density and size in terms of the average number of Cu atoms per cluster and we do not address cluster dimension or composition. We note that cluster compositions would require the definition of an interface and quantification of

trajectory artifacts. Similarly, a conversion to cluster dimension (in nm) would require either a quantitative analysis of trajectory aberrations or quantitative knowledge of the Cu cluster compositions from which one can derive the total number of atoms in each cluster and an equivalent cluster radius. Note that this calculation also requires an informed decision regarding the atomic density of the clusters.

Starting with the single operator dataset, the MSM method was applied using Cu as core (solute) atoms with no prior filtering. An order of four was selected to generate NND distributions. The distributions exhibited two humps corresponding to the matrix and the cluster concentrations. These were fitted with Gaussian functions and the intercept between the two functions determined the value of d_{\max} . The minimum number of solutes in a cluster, N_{\min} , was established as the largest cluster size detected in the random dataset. Five randomized distributions were generated and the N_{\min} was determined by averaging the N_{\min} values determined from each randomized dataset, and an uncertainty range (full range) was assigned to the number of clusters using the range of N_{\min} values. The d_{\max} values were between 1.0 and 1.3 nm, the N_{\min} values were between 8 and 12 Cu atoms.

In the case of the results reported by the multiple operators, Cu was also systematically chosen as the core atom. However, a broader range of values were selected for the different parameters. The k values were between 1 and 10, the d_{\max} values were between 0.7 and 1.52 nm, and N_{\min} values were between 5 and 13 Cu atoms. One should note that the values of k and d_{\max} are not independent, since, as k increases, so does d_{\max} . Three of the analyses relied on concentration thresholding with a threshold value between 2.3 and 4 at% Cu. These threshold values were determined by comparing the mass-randomized local concentration histogram with the real distribution.

The cluster number density measured by the single operator averaged over the 13 datasets was $(1.1 \pm 0.2) \times 10^{24}/\text{m}^3$ and the average density averaged over the 14 datasets analyzed by multiple operators was $(0.8 \pm 0.3) \times 10^{24}/\text{m}^3$ (Fig. 3b). Here the uncertainty is defined as one standard deviation of the distribution. The densities were calculated from the reported number of clusters divided by the estimated volume of the reconstructions that are calculated from the number of ranged ions in the volume and the detection efficiency of the instrument. The average sizes are also comparable for the single operator (60 ± 10 Cu atoms) and for the multiple operators (54 ± 23 Cu atoms), where the numbers of atoms were normalized by the detection efficiency of the instrument (Fig. 3c).

Ni-Si Clusters

In addition to Cu clusters, irradiation also induced the formation of dislocation loops decorated with Si and the formation and Ni-Si clusters. The latter is the focus of this section. The measured dataset concentrations of Ni and Si as reported by the participants were higher than that of Cu: 8.40 and 1.55 at%, respectively, with standard deviations of ± 0.43 at% and ± 0.07 at%, respectively.

In the case of the single operator, Ni, rather than Si, was chosen as the core atom. The cluster analysis with Si as the core atom would potentially identify both Ni-Si clusters and Si-decorated dislocation loops and introduce an additional step to separate the two population. Considering the low-density contrast between matrix and clusters and that the interface of the clusters is relatively wide, the difference between the Ni-rich clusters and matrix

Table 1. Summary of Reconstruction Parameters Used for Each APT Dataset.

Dataset	T (K)	Pulse amplitude (%)	Pulse frequency (kHz)	Detection rate ($100 \times$ atoms/pulse)	η	ICF_s	K_s	ICF_m	K_m
1	56	20	200	0.2	0.37	1.05	3.3	1.65	4.5
2	56	20	200	0.6	0.37	1.05	3.2	1.65	4.5
3	50	20	200	0.4	0.36	1.1	3.6	1.65	3.3
4	50	20	200	0.4	0.36	1.1	3.2	1.65	3.3
5	67	15	200	0.25	0.36	1.3	3.5	1.55	4.2
6	54	20	200	0.8	0.36	1.6	5.2	1.65	4.5
7	54	20	200	0.6	0.36	1.6	5.4	1.65	4.1
8	44	20	200	0.5	0.37	1.35	4.4	1.65	3.3
9	71	15	200	0.15	0.36	1.2	4.2	1.65	4
10	50	20	200	0.2	0.52	1.6	4.4	1.45	3.3
11	50	20	200	0.1	0.52	1.1	3.4	1.45	3.3
12	45	20	200	0.3	0.36	1.6	4.8	1.12	3.3
13	54	15	200	1.2	0.37	1.1	2.8	1.2	3.3
14	50	0.2–0.3 nJ	255	2.5–5.5 ^a	0.52	1.6	3.3	NA	NA

The subscript s is used to denote the single operator data and m for multiple operator data. η is the detection efficiency, ICF is the image compression factor, and K is the field factor. All participants used the default evaporation field value for Fe of 33 V/nm.

^aDetection rate was adjusted automatically to account for the increase in evaporation area during the analysis.

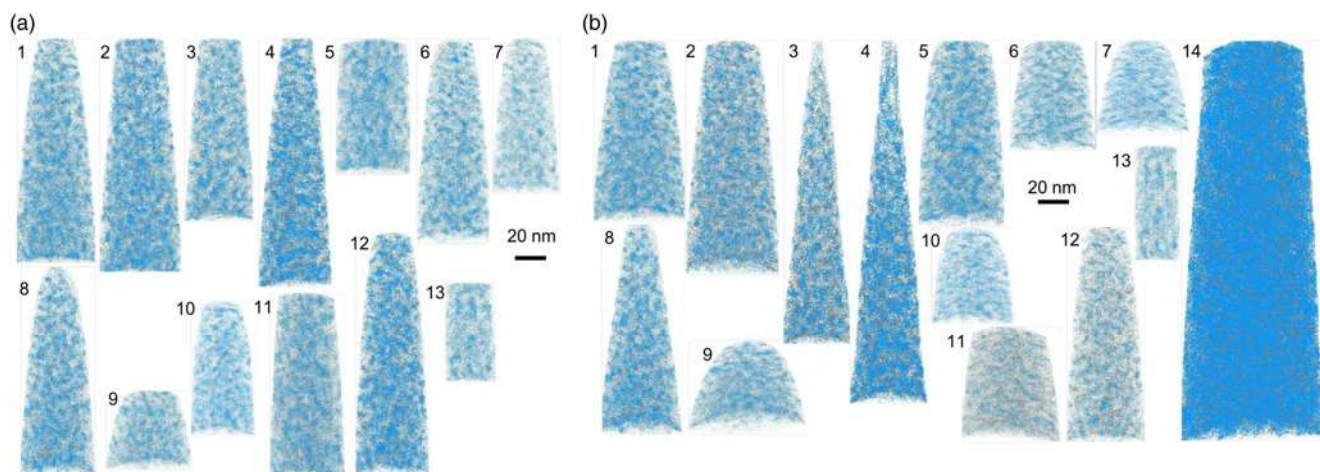


Fig. 2. Reconstructed volumes by (a) single and (b) multiple operators showing 100% of Si in blue and Cu in orange. Note that, in addition to differences in reconstruction parameters, the volumes selected for reconstruction may vary from one operator to the next.

cannot be well resolved by the traditional MSM approach. A filtering approach, adapted from Chen et al. (2014), was applied, based on the lower local Ni concentrations of nonclustered matrix Ni atoms. The threshold concentration, defined as the concentration at which the difference between the concentration distributions from the experimental and the random datasets becomes positive, was used to select Ni atoms with high Ni local concentrations. Values for the threshold concentrations were between 16 and 24 at% Ni. The order of ten was then used for cluster searching on the filtered data. The value of d_{max} , between 0.94 and 1.10 nm, was selected as the distance where the distribution of NNDs from the randomized filtered data becomes nonzero (Fig. 4a). Since the matrix has already been removed by setting the local concentration value above 16 at%, false clusters are

removed by N_{min} , based on the cluster size distribution. The value of N_{min} (typically smaller than 40 to 60 atoms) is chosen so that any cluster containing no Si atoms is excluded (vertical line in Fig. 4b). In addition, only clusters containing at least three Si atoms are counted. Finally, an additional visual inspection was conducted to remove the handful of potential large dislocation fragments, identified by their size and elongated aspect ratio. The Ni-to-Si ratios reported by the single operator were calculated from a cluster radial concentration profile. The interface between clusters and matrix was defined as the point where the Ni concentration is mid-point between the matrix concentration and the concentration at the center of the clusters. A sensitivity analysis would involve varying the threshold concentration and the values of d_{max} , N_{min} , and k . We note that there is a potential

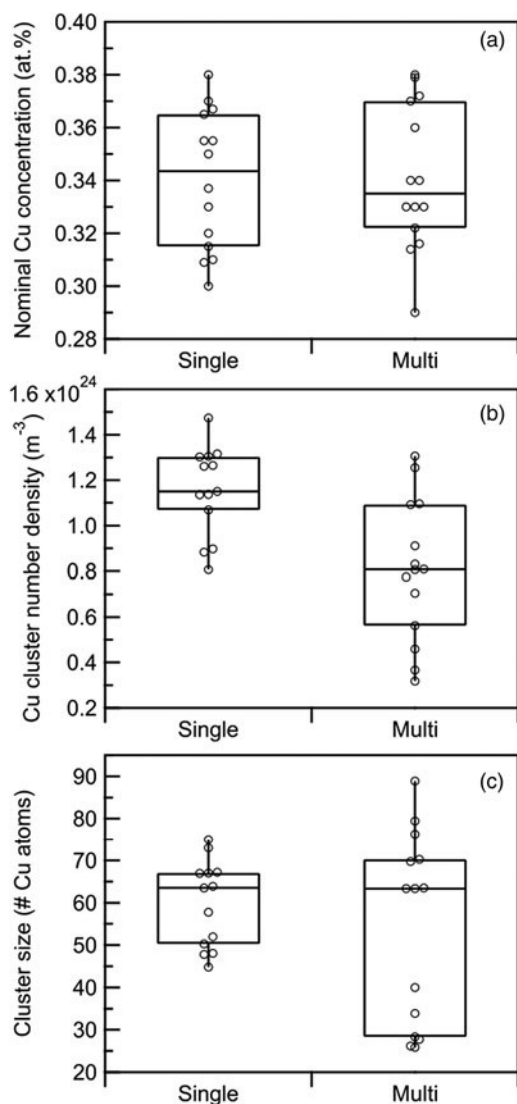


Fig. 3. (a) Measured Cu concentration in the reconstructed volumes. (b) Number density of identified Cu clusters. (c) Average size (expressed in number of Cu atom within each cluster) of identified Cu clusters. Note that all numbers have been adjusted to account for detection efficiency. The horizontal lines represent the mean values of the distributions and the boxes represent the interquartile ranges. The results for each dataset are included in Supplementary Appendix II.

significant uncertainty ($>20\%$) associated with the identification of the Ni clusters and therefore their number density, given the steepness of the dependence with some of these parameters.

In the case of multiple operators, four datasets were analyzed using concentration filtering (#5, 10, 11, 14), while the other ten were directly analyzed with the MSM method. In the case of the MSM method, participants used either Si, Ni, or Ni + Si as core atoms and the selected order values were either 1 or 10, the d_{\max} values were between 0.4 and 1.1 nm, and N_{\min} values between 15 and 110 Si, Ni, or Ni + Si atoms. When using one of the variations based on concentration thresholding, participants used Ni or Ni + Si atoms as core atoms with C_{th} values between 16 and 24 at% and N_{\min} values between 23 and 90 atoms.

The average number density of Ni-Si clusters for the single operator across all datasets is $9 \pm 1 \times 10^{23}/\text{m}^3$. For multiple operators, the average is $14 \pm 7 \times 10^{23}/\text{m}^3$. The distribution of reported cluster size exhibits two populations. The high number density

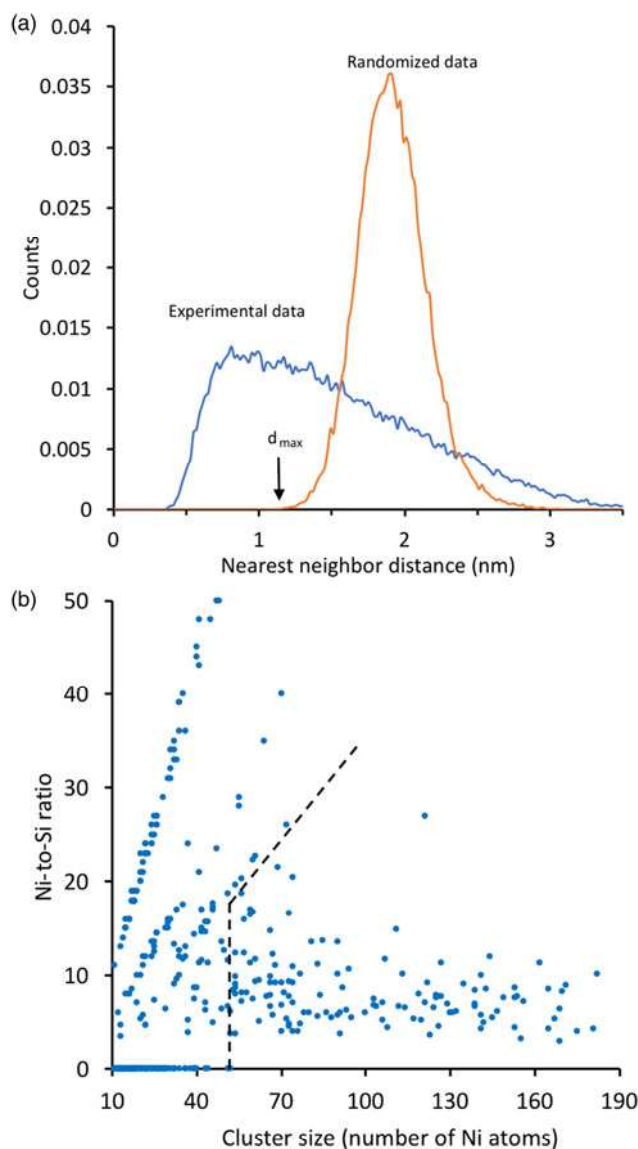


Fig. 4. (a) Nearest neighbor distributions with Ni as core atom after filtering and (b) selection of N_{\min} .

values ($>10^{24}/\text{m}^3$) tend to correspond to the analyses with direct application of the MSM method (Fig. 5). Exceptions are dataset #3 and #4 for which a small d_{\max} value of 0.4 nm was used, leading to a conservative estimate of the number of clusters. Among the analyses based on concentration filtering, the highest reported density (dataset #5) was obtained using a relatively small N_{\min} value (23) that could be associated with a generous identification of the clusters. When only considering results leveraging concentration filtering, the multiple operator average over the dataset falls to $1.0 \pm 0.5 \times 10^{24}/\text{m}^3$, versus $1.7 \pm 0.7 \times 10^{24}/\text{m}^3$ for direct application of MSM. The average size across datasets is 147 ± 13 Ni atoms for the single operator data, 310 ± 160 Ni atoms for all multiple operators results, and 240 ± 175 Ni atoms for multiple operators based on concentration filtering. The average Ni-to-Si ratio, defined here as the ratio of the total number of Ni atoms to the total number of Si atoms, is 3.0 ± 1 for the single operator data, and 2.3 ± 0.8 for all multiple operators results, and 2.3 ± 1 for multiple operators based on concentration filtering. Results are summarized in Figure 6. We note that the reported cluster

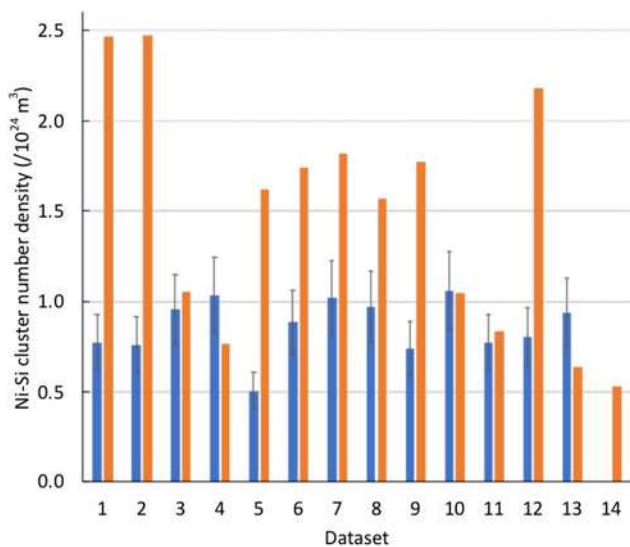


Fig. 5. Number density of identified Ni-rich clusters. The error bar was defined by the spread in number density when varying the N_{\min} to $N_{\min} \pm 5$. Here ± 5 was selected arbitrarily to illustrate the dependence with N_{\min} . Single operator data is in blue, multiple operator data is in orange.

sizes and Ni-to-Si ratios are less sensitive to the choice of the analysis method than is the cluster number density measurement.

Dislocation Loops

The most challenging aspect of the dataset was the analysis of dislocation loops from the observed Si segregation patterns. Since the focus of this interlaboratory study is the use of the MSM or LCT methods, participants attempted to analyze dislocation loops via these methods, while recognizing that they may not be appropriate for such analysis. The single participant followed the method described in Chen et al. (2014). Two users from the set of multiple operators reported numbers from dislocation loop analysis, in both cases based on the clustering analysis of Si or Ni and Si followed by visual filtering. Results are summarized in Figure 7.

Discussion

This experimental interlaboratory study on cluster analysis in a proton irradiated 304 stainless steel builds upon discussions and experience established in an earlier interlaboratory study that focused on the analyses of synthetic data and led to a first set of recommendations and methods summarized in Marquis et al. (2017). Considering the discussions among participants and the experience gained, this study revisits the analysis of real experimental data where different sources of variability might contribute to measurement scatter. These include the material itself (compositional inhomogeneity and fluctuations), instrumentation sources (detector technology and data pre-processing as performed by manufacturer), acquisition conditions and specific evaporation conditions (crystallography of selected grains, sample temperature, and effect on surface migration), and operator sources (specimen preparation, data collection conditions, reconstruction, mass ranging, and data analysis procedure). Here, crystallographic effects were minimized by producing all of the specimens from the same grain. The role of instrumentation was also minimized, with all data collected on similar

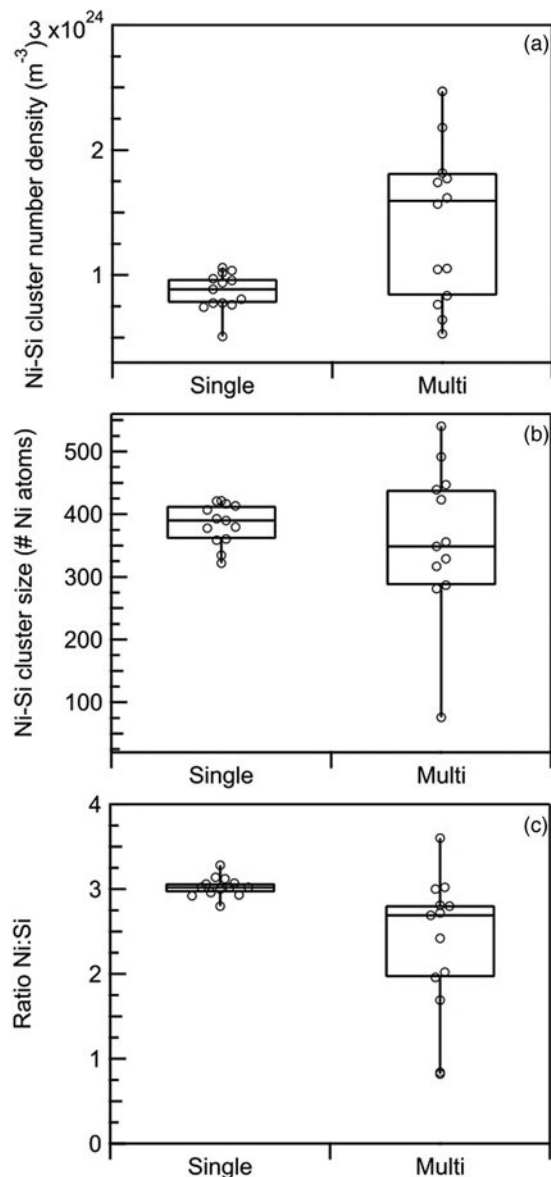


Fig. 6. (a) Number density of identified Ni-rich clusters. (b) Average size (number of Ni atom inside) of identified Ni clusters. (c) Ni-to-Si ratio of identified Ni clusters. The horizontal lines represent the mean values of the distributions and the boxes represent the interquartile ranges. The results for each dataset are included in Supplementary Appendix II.

instruments, LEAP 4000 XHR or 3000X HR, with the exception of two datasets collected on a similar LEAP 5000 XR. The present study was therefore designed to emphasize operator sources, specifically, reconstruction, mass ranging, and data analysis procedure.

Reconstruction and scaling of the dataset introduces some variability in the cluster detection, which should not be too surprising since the relative distances between atoms are modified. The error introduced on the measurement of the number of Cu clusters is of the order of 6%—smaller than the variability associated with the selection of the data analysis parameters. The error was estimated through the following example, where one of the datasets was reconstructed using two different sets of parameters (Fig. 8a). The nearest neighbor distribution of Cu is not modified significantly yielding values of d_{\max} of 1.18 and 1.13 nm (Fig. 8b) and the detected numbers of clusters are 173 ± 19 and 163 ± 16 ,

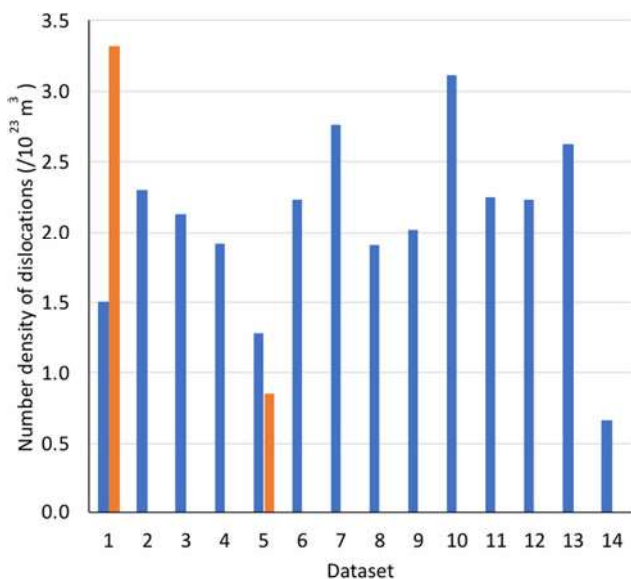


Fig. 7. Dislocation loop number density. Single operator results are in blue, multiple operator data is in orange.

respectively (Fig. 8c), where the range values correspond to changing N_{\min} by ± 1 .

Mass ranging has a stronger effect on cluster identification. As an extreme case, we compare the results from the same dataset analyzed with either ranges extending to the noise level, or with ranges defined by the full width at half maximum of each peak (Fig. 9a). Significantly different measured Cu concentrations result: 0.37 and 0.23 at%, respectively. While the nearest neighbor distribution changes somewhat with slightly different selected d_{\max} values and the N_{\min} values are not affected, the detected number of clusters changes more significantly: 173 ± 19 and 135 ± 18 (Fig. 9b).

Differences in mass ranging strategies among the participants were not as dramatic as in the example above. Nonetheless, variations in ranging introduced nonnegligible variability in the reported number of clusters. To illustrate this point, a third set of Cu cluster analyses was conducted by the single operator using the reconstructed datasets as generated by the single operator and the range files provided by the multiple operators. This third set aimed at minimizing the variability coming from reconstruction and cluster finding methods. The original single operator analysis, where ranges were systematically defined so as to select the portion of the peak above the noise level, yielded a distribution of number densities that varied over a factor of two with a standard deviation of $\sim 17\%$. The multiple operator results varied by a factor of four with a standard deviation of $\sim 39\%$. The second set of single operator analyses, using range files that varied significantly in their definitions, was tighter, with results varying within 40% and a standard deviation of 12%. Comparing the two sets of single operator analyses that were conducted using the same clustering analysis approach, the use of different range files resulted in variations in the reported number density of clusters by up to 33% for a given dataset.

Regarding the overall results, the first single operator results were systematically higher than the measurements from the multiple operators and for the most part higher than the second single operator results. We cannot exclude a potential bias of the single operator to inadvertently “fit” subsequent measurement to the

initial ones. However, a similar dependence of the cluster number density with Cu concentration within the dataset is found in both sets of analyses (Fig. 10). Such a dependence may be rationalized by an increase in driving force for clustering associated with a higher solute concentration. This dependence is significantly less expressed in the second single operator data (in green in Fig. 10), which we attribute to the superimposition of two independent contributions with high variabilities: ranging and cluster detection. While the first single and the multiple operator datasets suggest a discrepancy of factor 2 in the assessed Cu cluster number densities, the differences for a given dataset suggest discrepancies up to a factor 4. The latter is a more relevant measure of the overall variability between operators and is dominated by the variability stemming from the cluster detection algorithm and parameter choices.

The analysis of Cu clusters shows that the MSM works well and is even able to detect subtle dependencies with minor solute concentrations. The IPM method also provides consistent results. The influence of local composition on somewhat larger precipitates has been highlighted before in reactor pressure vessel steels (Wells et al., 2014). Here the dependence with Cu concentration is more subtle and was resolved. The preliminary comparison of the voltage and laser mode data suggest that any potential effect of the data acquisition conditions is within the range of variability originating from other common sources: local concentration, analysis methods, and parameter selection.

Regarding the analysis of Ni–Si clusters, additional considerations come into play. One could choose Si, Ni, or Ni + Si as core atoms. The use of the MSM method with Si as core atoms posed some challenges. The segregation of Si to dislocations potentially led to the detection of additional clusters that could explain the systematic higher number density of clusters as well as the low Ni-to-Si ratio reported by the MSM method. The selection of Ni or Ni + Si required the use of density filtering, since Ni or Ni + Si remain relatively concentrated away from the clusters. Similarly to the Cu clusters, the reported number density varied by up to factor 5. We note here that the MSM tends to predict twice as many clusters as a filtering method.

The limited clustering analysis steps, within the common IVAS software package, can limit the exploration of alternative methods. However, open-access platforms, e.g. 3Depict (Haley, 2010), and the increasing number of freely accessible codes and methods, e.g. London (2016), should lower the barrier of entry for new users as well as increase the range of analysis methods available to all. The analysis of solute clustering in APT data would certainly benefit from more advanced cluster search algorithms that are less dependent on user input and more robust with respect to density variations. It is important to note the existence of previously published clustering data that might have resulted from the use of methods that were either not appropriate for the considered microstructures or biased by the complexity of the analyzed microstructures.

Finally, it is clear that the analysis of dislocation loops beyond qualitative observations and statements requires additional work, primarily in the development of topological analysis methods. We would also like to note that the selected microstructure was a particularly challenging one. In the case of neutron-irradiated 304 steel, some of the microstructural features typically develop with larger characteristic length scales that would significantly ease data analysis and interpretation. Yet other features, such as Cu-rich or Al-rich clusters remain small and require careful analyses. Other materials and microstructures, such as some reactor

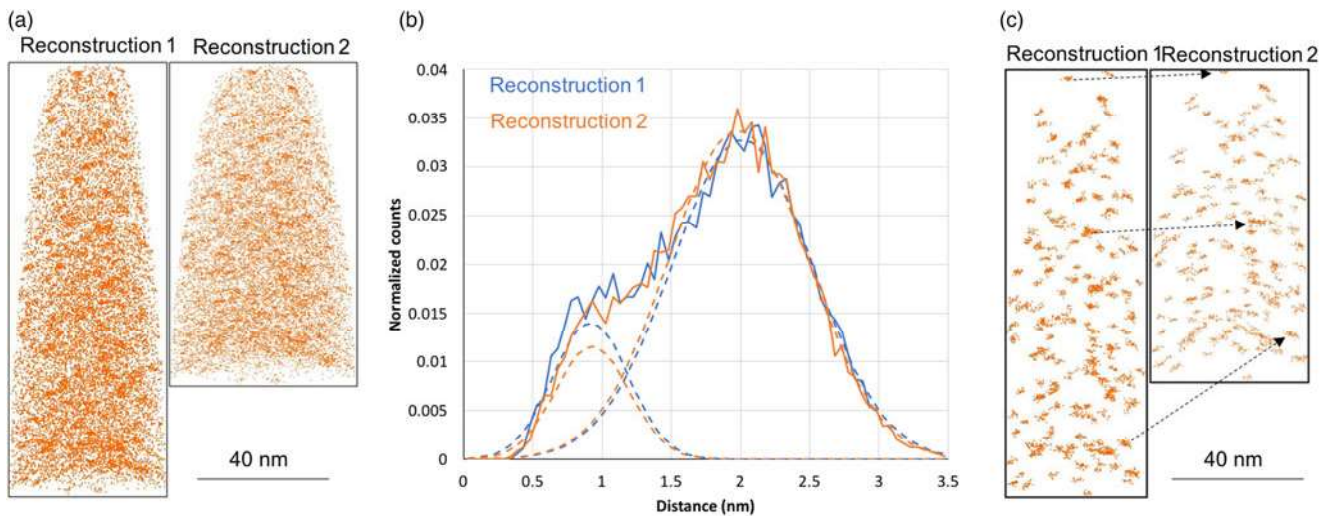


Fig. 8. (a) Two reconstructions of the same dataset; (b) resulting nearest neighbor distributions for Cu atoms; and (c) identified Cu clusters using the method defined by the single operator. Arrows show the correspondence between clusters.

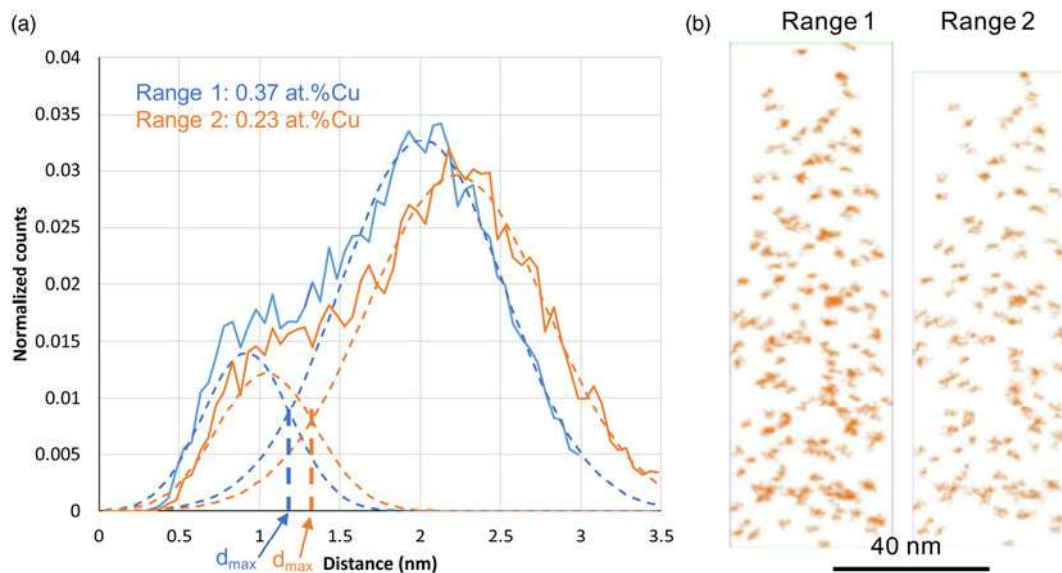


Fig. 9. (a) Nearest neighbor distributions for Cu atoms generated from the same dataset using two different ranging strategies; and (b) resulting Cu clusters using the method defined by the single operator.

pressure vessel steels, exhibit fine scale clustering where the results of this interlaboratory study are highly relevant.

Conclusions and Recommendations

As highlighted in many existing publications, the analysis of solute clustering is nontrivial. From this interlaboratory study, two main sources of uncertainty need to be considered carefully. The interpretation of the mass spectrum via “ranging”, as well as the user selection of parameters inherent to the MSM and LCT methods, can influence greatly the outcome of the cluster analysis to the extent of a factor 3 on the detected number density of Cu clusters. The use of the MSM remains problematic for concentrated solutes, such as Ni and Si in a typical 304 stainless steel.

The “correct” cluster distribution is an unknown piece of information that cannot be represented via a single value, as often done in the existing APT literature, but rather via a range

defined by an uncertainty level. Consequently, following similar efforts within the APT community (Blum et al., 2017), we emphasize again the need for thorough reporting of the analysis methods, which includes detailed justification of the method and selection of relevant parameters. This information is not only essential for the reproducibility of the results, but also ensures that the data presented, including its likely biases, may be accurately interpreted by future researchers. Minimum information includes:

- Reconstruction method and parameter values (e.g., software version and values for ICF, K , and the constant evaporation field, F).
- Mass spectrum and range file including whether any peak overlaps are present and how they are accounted for with overlap diagrams.
- Name of method with specific algorithm made available.

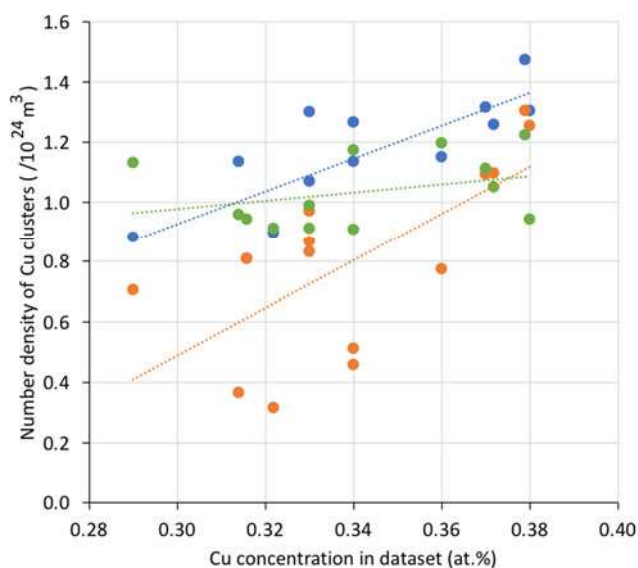



Fig. 10. Dependence of cluster number density with Cu concentration. Single operator data are in blue, multiple operator data in orange, and green corresponds to the single operator re-analysis using mass ranges defined by the multiple operators. The x-axis represents the values of the Cu concentration in the as reported by the multiple operators. The same trend applies if the single operator values are selected.

- Justification as to why the selected method applies.
- Values of all relevant parameters.
- Justification for the parameter values that were selected.
- Sensitivity analysis and estimation of variability with parameter values.

An example of how such information may be organized and presented is provided as a downloadable supplementary document (Supplementary material).

Supplementary material. The supplementary material for this article can be found at <https://doi.org/10.1017/S1431927618015581>.

Author ORCIDs.  Andrew London, 0000-0001-6959-9849; Emmanuelle Marquis, 0000-0002-6476-2835; Mattias Thuvander, 0000-0002-6097-6895.

Acknowledgments. The authors acknowledge the voluntary participation by most members of the APT interlaboratory study, financial support of EPRI and EDF-MAI for the analysis of the aggregate results and preparation of the samples at the University of Michigan, Gary Was at the University of Michigan for providing the proton irradiated sample, and Allen Hunter at the Michigan Center for Materials Characterization for preparation of the specimens that were sent to the participants. DKS and JW acknowledge financial support from the US Department of Energy, Office of Science, Basic Energy Sciences. AE, CH, and BR acknowledge financial support from the Région Haute-Normandie, the Métropole Rouen Normandie, the CNRS via LABEX EMC and the French National Research Agency as a part of the program “Investissements d’avenir” with the reference ANR-11-EQPX-0020.

References

Auger P, Pareige P, Welzel S and Van Duysen JC (2000). Synthesis of atom probe experiments on irradiation-induced solute segregation in French ferritic pressure vessel steels. *J Nucl Mater* **280**(3), 331–344.

Blavette D and Chambreland S (1986). A statistical model for deriving microstructure parameters of finely dispersed systems from atom-probe analyses. *J Phys Colloq* **47**(C7), C7–503.

Blum TB, Darling JR, Kelly TF, Larson DJ, Moser DE, Perez-Huerta A, Prosa TJ, Reddy SM, Reinhard DA, Saxey DW, Ulfing RM and

Valley JW (2017). Best practices for reporting atom probe analysis of geological materials. In *Microstructural Geochronology: Planetary Records Down to Atom Scale*. Moser DE, Corfu F, Darling JR, Reddy SM and Tait K. Wiley, pp. 369–373.

Ceguerra AV, Moody MP, Stephenson LT, Marceau RKW and Ringer SP (2010). A three-dimensional Markov field approach for the analysis of atomic clustering in atom probe data. *Philos Mag* **90**(12), 1657–1683.

Cerezo A and Davin L (2007). Aspects of the observation of clusters in the 3-dimensional atom probe. *Surf Interface Anal* **39**, 184–188.

Chen Y, Chou PH and Marquis EA (2014). Quantitative atom probe tomography characterization of microstructures in a proton irradiated 304 stainless steel. *J Nucl Mater* **451**(1–3), 130–136.

Couturier L, De Geuser F and Deschamps A (2016). Direct comparison of Fe–Cr unmixing characterization by atom probe tomography and small angle scattering. *Mater Charact* **121**, 61–67.

CVL (2016). CVL: Characterization Virtual Laboratory. Monash University. Available at <https://www.massive.org.au/cvl/cvl-workbenches/atom-probe-workbench>.

De Geuser F, Lefebvre W and Blavette D (2006). 3D atom probe study of solute atoms clustering during natural ageing and pre-ageing of an Al–Mg–Si alloy. *Philos Mag Lett* **86**(4), 227–234.

Edmondson PD, Miller MK, Powers KA and Nanstad RK (2016). Atom probe tomography characterization of neutron irradiated surveillance samples from the R. E. Ginna reactor pressure vessel. *J Nucl Mater* **470**, 147–154.

Gault B, Danoix F, Hoummada K, Mangelinck D and Leitner H (2012a). Impact of directional walk on atom probe microanalysis. *Ultramicroscopy* **113**, 182–191.

Gault B, Moody MP, Cairney JM and Ringer SP (2012b). *Atom Probe Microscopy*. New York: Springer-Verlag.

Gurovich B, Kuleshova E, Shtrombakh Y, Fedotova S, Maltsev D, Frolov A, Zabusov O, Erak D and Zhurko D (2015). Evolution of structure and properties of VVER-1000 RPV steels under accelerated irradiation up to beyond design fluences. *J Nucl Mater* **456**, 23–32.

Haley D (2010). 3Depict—Visualisation and Analysis for Atom Probe. Available at <http://threedepict.sourceforge.net/>.

Heinrich A, Al-Kassab TA and Kirchheim R (2003). Investigation of the early stages of decomposition of Cu–0.7 at% Fe with the tomographic atom probe. *Mater Sci Eng A* **353**(1–2), 92–98.

Hellman OC, Vandenbroucke JA, Rüsing J, Isheim D and Seidman DN (2000). Analysis of three-dimensional atom probe data by the proximity histogram. *Microsc Microanal* **6**, 437–444.

Hyde JM, Cerezo A and Williams TJ (2009). Statistical analysis of atom probe data: Detecting the early stages of solute clustering and/or co-segregation. *Ultramicroscopy* **109**(5), 502–509.

Hyde JM, DaCosta G, Hatzoglou C, Weekes H, Radiguet B, Styman PD, Vurpillot F, Pareige C, Etienne A, Bonny G, Castin N, Malerba L and Pareige P (2017). Analysis of radiation damage in light water reactors: Comparison of cluster analysis methods for the analysis of atom probe data. *Microsc Microanal* **23**(2), 366–375.

Hyde JM, Marquis EA, Wilford KB and Williams TJ (2011). A sensitivity analysis of the maximum separation method for the characterisation of solute clusters. *Ultramicroscopy* **111**(6), 440–447.

Jaegle EA, Choi PP and Raabe D (2014). The maximum separation cluster analysis algorithm for atom-probe tomography: Parameter determination and accuracy. *Microsc Microanal* **20**, 1662–1671.

Jiao Z and Was GS (2011). Impact of localized deformation on IASCC in austenitic stainless steels. *J Nucl Mater* **408**(3), 246–256.

Kolli RP and Seidman DN (2007). Comparison of compositional and morphological atom-probe tomography analyses for a multicomponent Fe–Cu steel. *Microsc Microanal* **13**, 272–284.

Kuramoto A, Toyama T, Nagai Y, Inoue K, Nozawa Y, Hasegawa M and Valo M (2013). Microstructural changes in a Russian-type reactor weld material after neutron irradiation, post-irradiation annealing and re-irradiation studied by atom probe tomography and positron annihilation spectroscopy. *Acta Mater* **61**(14), 5236–5246.

Lefebvre W, Philippe T and Vurpillot F (2011). Application of Delaunay tessellation for the characterization of solute-rich clusters in atom probe tomography. *Ultramicroscopy* **111**(3), 200–206.

- Lefebvre W, Vurpillot F and Sauvage X** (2016). *Atom Probe Tomography, Put Theory Into Practice*, Elsevier.
- London A** (2016). AtomProbeLab: Matlab-based analysis of Atom Probe Data. Available at <https://sourceforge.net/projects/atomprobelab/>.
- Marceau RK, Stephenson LT, Hutchinson CR and Ringer SP** (2011). Quantitative atom probe analysis of nanostructure containing clusters and precipitates with multiple length scales. *Ultramicroscopy* **111**(6), 738–742.
- Marquis EA, Araullo-Peters V, Dong Y, Etienne A, Fedotova S, Fujii K, Fukuya K, Kuleshova E, Lopez A, London A, Lozano-Perez S, Nagai Y, Nishida K, Radiguet B, Schreiber D, Soneda N, Thuvander M, Toyama T, Sefta F and Chou P** (2017). On the use of density-based algorithms for the analysis of solute clustering in atom probe tomography data. Proceedings of the 18th International Conference on Environmental Degradation of Materials in Nuclear Power Systems—Water Reactors. The Minerals, Metals and Materials Series. Springer, Cham.
- Meslin E, Lambrecht M, Hernández-Mayoral M, Bergner F, Malerba L, Pareige P, Radiguet B, Barbu A, Gómez-Briceño D, Ulbricht A and Almazouzi A** (2010). Characterization of neutron-irradiated ferritic model alloys and a RPV steel from combined APT, SANS, TEM and PAS analyses. *J Nucl Mater* **406**(1), 73–83.
- Meslin E, Radiguet B and Loyer-Prost M** (2013). Radiation-induced precipitation in a ferritic model alloy: An experimental and theoretical study. *Acta Mater* **61**(16), 6246–6254.
- Miller MK and Hetherington MG** (1991). Local magnification effects in the atom probe. *Surf Sci* **246**, 442–449.
- Miller MK, Powers KA, Nanstad RK and Efsing P** (2013). Atom probe tomography characterizations of high nickel, low copper surveillance RPV welds irradiated to high fluences. *J Nucl Mater* **437**(1–3), 107–115.
- Miller MK and Russell KF** (2007). Embrittlement of RPV steels: An atom probe tomography perspective. *J Nucl Mater* **371**(1), 145–160.
- Miller MK, Russell KF, Kocik J and Keilova E** (2000). Embrittlement of low copper VVER 440 surveillance samples neutron-irradiated to high fluences. *J Nucl Mater* **282**(1), 83–88.
- Moody MP, Stephenson LT, Ceguerra AV and Ringer SP** (2008). Quantitative binomial distribution analyses of nanoscale like-solute atom clustering and segregation in atom probe tomography data. *Microsc Res Technol* **71**(7), 542–550.
- Pareige P, Stoller RE, Russell KF and Miller MK** (1997). Atom probe characterization of the microstructure of nuclear pressure vessel surveillance materials after neutron irradiation and after annealing treatments. *J Nucl Mater* **249**(2–3), 165–174.
- Radiguet B, Barbu A and Pareige P** (2007). Understanding of copper precipitation under electron or ion irradiations in FeCu 0.1 wt% ferritic alloy by combination of experiments and modelling. *J Nucl Mater* **360**, 104–117.
- Rose DJ** (1956). On the magnification and resolution of the field emission electron microscope. *J Appl Phys* **27**(3), 215–220.
- Saxey DW** (2011). Correlated ion analysis and the interpretation of atom probe mass spectra. *Ultramicroscopy* **111**(6), 473–479.
- Shu S, Wirth BD, Wells PB, Morgan DD and Odette GR** (2018). Multi-technique characterization of the precipitates in thermally aged and neutron irradiated Fe–Cu and Fe–Cu–Mn model alloys: Atom probe tomography reconstruction implications. *Acta Mater* **146**, 237–252.
- Stephenson LT, Moody MP, Liddicoat PV and Ringer SP** (2007). New techniques for the analysis of fine-scaled clustering phenomena within atom probe tomography (APT) data. *Microsc Microanal* **13**(6), 448–463.
- Styman PD, Hyde JM, Parfitt D, Wilford K, Burke MG, English CA and Efsing P** (2015). Post-irradiation annealing of Ni–Mn–Si-enriched clusters in a neutron-irradiated RPV steel weld using atom probe tomography. *J Nucl Mater* **459**, 127–134.
- Styman PD, Hyde JM, Wilford K and Smith GDW** (2013). Quantitative methods for the APT analysis of thermally aged RPV steels. *Ultramicroscopy* **132**(0), 258–264.
- Takeuchi T, Kuramoto A, Kameda J, Toyama T, Nagai Y, Hasegawa M, Ohkubo T, Yoshiie T, Nishiyama Y and Onizawa K** (2010). Effects of chemical composition and dose on microstructure evolution and hardening of neutron-irradiated reactor pressure vessel steels. *J Nucl Mater* **402**(2), 93–101.
- Thompson K, Lawrence D, Larson DJ, Olson JD, Kelly TF and Gorman B** (2007). *In situ* site-specific specimen preparation for atom probe tomography. *Ultramicroscopy* **107**(2–3), 131–139.
- Toyama T, Kuramoto A, Nagai Y, Inoue K, Nozawa Y, Shimizu Y, Matsukawa Y, Hasegawa M and Valo M** (2014). Effects of post-irradiation annealing and re-irradiation on microstructure in surveillance test specimens of the Loviisa-1 reactor studied by atom probe tomography and positron annihilation. *J Nucl Mater* **449**, 207–212.
- Toyama T, Nagai Y, Tang Z, Hasegawa M, Almazouzi A, van Walle E and Gerard R** (2007). Nanostructural evolution in surveillance test specimens of a commercial nuclear reactor pressure vessel studied by three-dimensional atom probe and positron annihilation. *Acta Mater* **55**(20), 6852–6860.
- Vaumousse D, Cerezo A and Warren PJ** (2003). A procedure for quantification of precipitates microstructures from three-dimensional atom probe data. *Ultramicroscopy* **95**, 215–221.
- Vurpillot F, Bostel A and Blavette D** (2000a). Trajectory overlaps and local magnification in three-dimensional atom probe. *Appl Phys Lett* **76**(21), 3127–3129.
- Vurpillot F, Bostel A, Cadel E and Blavette D** (2000b). The spatial resolution of 3D atom probe in the investigation of single-phase materials. *Ultramicroscopy* **84**(3–4), 213–224.
- Vurpillot F, De Geuser F, Da Costa G and Blavette D** (2004). Application of Fourier transform and autocorrelation to cluster identification in the three-dimensional atom probe. *J Microsc* **216**, 234–240.
- Waugh AR, Boyes ED and MJ S** (1876). Investigations of field evaporation with a field-desorption microscope. *Surf Sci* **69**(1), 109–142.
- Wells PB, Yamamoto T, Miller B, Milot T, Cole J, Wu Y and Odette GR** (2014). Evolution of manganese–nickel–silicon-dominated phases in highly irradiated reactor pressure vessel steels. *Acta Mater* **80**, 205–219.
- Williams CA, Haley D, Marquis EA, Smith GD and Moody MP** (2013). Defining clusters in APT reconstructions of ODS steels. *Ultramicroscopy* **132**, 271–278.
- Zelenty J, Dahl A, Hyde J, Smith GD and Moody MP** (2017). Detecting clusters in atom probe data with Gaussian mixture models. *Microsc Microanal* **23**(2), 269–278.